The Excited-State Symmetry Characteristics of Platinum Phenylacetylene Compounds

Luke A. Emmert, Wonsook Choi, Jason A. Marshall, Jing Yang, Lauren A. Meyer, and James A. Brozik*

Department of Chemistry, The University of New Mexico, Albuquerque, New Mexico 87131

Received: August 5, 2003; In Final Form: October 21, 2003

$[Pt((^nBu)_3P)_2(ethynylbenzene)_2]$ and $[Pt((^nBu)_3P)_2(1,4\text{-}diethynylbenzene)_2]$, which possess D_{2h} micro-symmetry in their ground states, were studied at 77 K by time-resolved infrared (TRIR), FTIR, steady-state emission, and time-resolved photoluminescence spectroscopies. The primary luminescence peaks are at 22 573 cm^{-1} and 20 408 cm^{-1}, respectively, with additional resolved structure from both phenyl ring and ethynyl vibrations. A quantum chemical modeling study showed that the HOMO is composed of conjugated π-obitials, which include contribution from the d_{xy} orbital on the platinum metal, while the LUMO consists of only the ligand π^* antibonding orbitals, thus the excitation is a mixture of $\pi\pi^*$ and MLCT. From the results of the TRIR study and from group theoretical requirements, it has been concluded that the excitation in the lowest triplet manifold is confined to one ligand, resulting in a reduction of symmetry to C_{2v}. For the ethynylbenzene compound, the lowest energy grow-in in the TRIR spectrum is in the range of a stretching vibration for a carbon−carbon double bond. In the 1,4-diethynylbenzene compound, the low-energy grow-in in the TRIR spectrum is intermediate between a doubly and triply bound carbon stretch. An explanation of the localization is presented through a coupling of the lowest energy $^3B_{3u}$ electronic manifold to a B_{3u} anti-symmetric ethynyl stretch on the peripheral ligands.

I. Introduction

Conjugated molecules and polymers with transition metals incorporated directly into the backbone have been the subject of intense study for a number of years.[1−9] This interest lies mainly in the fact that the incorporation of these metals into molecules and polymers relaxes the spin selection rules for phosphorescence through spin−orbit coupling. Such a property has proven to be quite important in the design of highly efficient next-generation light-emitting diodes in which the normally nonemissive triplet excitons emit light because of the relaxed selection rule.[10,11] Of particular interest in this regard is the family of organometallic molecules, oligomers, and polymers comprised of Pt(II), Pd(II), or Ni(II) with alkynyl bridging ligands.[10,11] This family is unique in that the π-orbitals on the ligands are fully conjugated with the d_{xy} orbitals of the metal sublattice. This creates favorable structural and electronic conditions for fast electron/hole or energy migration, which is necessary for efficient electron−hole recombination and the regeneration of the ground state through luminescence, no matter the spin multiplicity. Recently, particular interest has been paid toward understanding the extent of localization in the lowest emitting triplet manifold in this family of materials and a consensus seems to be taking shape. Both luminescence and polarized time-resolved transient absorption spectroscopy seem to show that the lowest triplet is localized on one or two repeat units while the lowest singlet and higher lying triplets are delocalized over several repeat units.[12−14] While these studies provide some compelling evidence of a localized excited triplet state in oligomers and polymers, there has yet to be a study that directly probes symmetry breaking in even the simplest members of this family of molecules.

This article explores the symmetry properties of the singlet ground state and lowest excited triplet manifold of states for $[Pt((^nBu)_3P)_2(ethynylbenzene)_2]$ and $[Pt((^nBu)_3P)_2(diethynylbenzene)_2]$ (abbreviated as Pteb and Ptdeb, respectively; see Figure 1 for structure and symmetry axis). This study makes use of time-resolved infrared spectroscopy (TRIR) to directly probe the structural and excited-state electronic symmetry of Pteb and Ptdeb while a quantum chemical modeling study has yielded a molecular orbital picture of the lowest excited triplet manifold and has aided in the assignments of the normal modes for the vibrations associated with the carbon−carbon triple bonds.

II. Experimental Section

A. Synthesis, Materials, and Sample Preparation. $Pt((^nBu)_3P)_2Cl_2$, Pteb, and Ptdeb were all synthesized from literature methods.[15,16] $K_2[PtCl_4]$, $(^nBu)_3P$, CuI, $NH(C_2H_5)_2$, and ethynylbenzene were all purchased from Aldrich Chemical Co. and used as received. Diethynylbenzene was purchased from TCI chemical and also used as received. All solvents were reagent grade and freshly distilled. Pteb and Ptdeb were purified first by flash chromatography, using alumina to remove excess CuI catalyst, followed by size exclusion chromatography, utilizing a sephadex LH-20 gel with THF as the eluent.

Samples suitable for spectroscopic study were prepared as poly(methyl methacrylate) (PMMA) films from freshly distilled reagent grade CH_2Cl_2. The PMMA had a molecular weight of ∼120 000 g/mol, was purchased from Aldrich Chemical Co. and was used as received. The films were prepared by dissolving ∼3 mg of the purified compound and 100 mg of PMMA in CH_2Cl_2 from which a plastic film was cast. For 77 K TRIR

* Author to whom correspondence should be addressed at The University of New Mexico, Department of Chemistry, Clark Hall Room 103, Albuquerque, NM 87131. E-mail: brozik@unm.edu.

10.1021/jp036309x CCC: $25.00 © 2003 American Chemical Society
Published on Web 12/02/2003

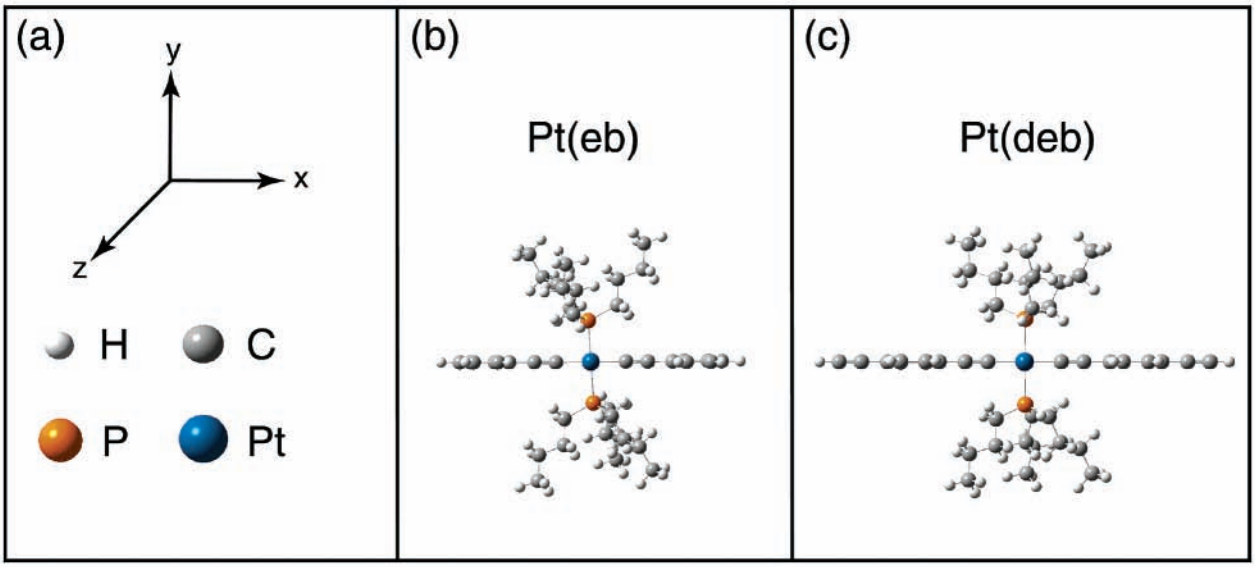

Figure 1. (a) Coordinate system used in theoretical study. SCF geometry-optimized molecular structures for (b) Pteb and (c) Ptdeb.

and luminescence studies, thin films of PMMA were prepared by casting the solution in shallow aluminum molds and allowing them to dry (~24 h) in air. The resultant thin films, which were delaminated after drying, had an average thickness of ~90 μm. The exact concentration of Pt compound in PMMA was adjusted so that the thin films had an average maximum IR absorbance of ~0.3 for the antisymmetric ethynyl stretch (vide infra) at 77 K. Samples suitable for ground-state FTIR experiments, in which the samples and reference backgrounds need to be the same thickness, were prepared by spin coating onto CaF_2 optical flats using a spin coater (Headway Inc. Model 1-EC101D-R790). Since these films were much thinner than the delaminated films described above, the optical absorbance was considerably smaller.

B. Spectroscopic Measurements. Steady-state emission spectra were obtained from samples mounted onto a custom-made sample holder, immersed directly into a bath of liquid nitrogen inside a quartz optical dewar. The excitation source was a 150 W Xe arc lamp that had been filtered with a combination of a $CuSO_4$ water filter and a UV band-pass filter to isolate a broad UV band peaking at 360 nm and focused directly onto the sample with a spherical quartz lens. The emitted light was monitored at 90° to the excitation beam, filtered through a 33 M KNO_2 filter (to remove scattered UV radiation), dispersed by an Acton 500i monochromator, and detected by a thermoelectrically cooled Hamamatsu R943-02 photomultiplier. The detector signal was passed through a wide-band preamplifier and fed to a Stanford Research Systems SR400 photon counter. Data were transferred to a PC for further manipulation. All spectra were corrected against a quartz-tungsten-halogen spectral irradiance standard lamp (Oriel Inc.).

For luminescence decay-time measurements at 77 K, the sample preparation method and detection system were as described above. The excitation source was the tripled output of a Nd:YAG laser (Continuum Minilite, 355 nm, 4 ns pulse width, 1 μJ pulse energy). An optical trigger synchronized the photon counter to the pulse train. The data were transferred to a PC for further analysis. All data reduction was achieved by means of a curve-fitting program (IGOR, Wavemetrics Inc.).

Low-temperature FTIR spectra were measured with a Nicolet Nexus 870 FTIR spectrophotometer. Samples were placed across a 3 mm hole drilled into a custom-made bronze sample holder that was subsequently attached to the thermal base of a 77 K cryostat (Janis Inc., model VPF-100). The cryostat was equipped with CaF_2 windows for both UV−Visible and IR experiments. The temperature was monitored with a calibrated silicon cryodiode (Lake Shore Cryotronics Inc., model DT-470-SC-13-1.4L) and controlled with a temperature controller (Lake Shore Cryotronics Inc., model 330). The cryostat was mounted directly into the sample compartment of the spectrophotometer via a custom-made mounting plate and aligned with a mechanical stage. All spectra were recorded at 8 cm^{-1} resolution with a liquid nitrogen cooled MCT detector.

For TRIR experiments, samples were mounted and cooled to 77 K in the Janis cryostat as described above. The entire TRIR spectroscopic experiment was sealed around the cryostat and purged with a continual stream of dry N_2. Electronic excitation was achieved by the tripled output of a Nd:YAG laser (Continuum Minilite, 355 nm, 4 ns pulse width, 50 μJ pulse energies) and transient IR signatures were probed with a commercial Step-Scan FTIR (SS-FTIR; Nicolet Nexus 870). Care was taken to overlap the excitation pulse with the IR probe (3 mm diameter). The spectral range of the IR probe was limited by a long pass filter (Janos F1305L300) and the CaF_2 windows of the Janis cryostat (spectral range: 3200 cm^{-1} to 1111 cm^{-1}). Timing between the interferometer and the laser was achieved with an optical trigger (photodiode, ThorLabs model DET210), and the entire time domain was recorded with a 100 MHz digital oscilloscope (Gage, model 12 100-1M). In the SS-FTIR spectroscopic study the moveable mirror of the interferometer was moved stepwise in 1.264 μm increments. The mirror was held stationary at each position while the data were collected. Two sets of data were acquired after each mirror step: one from the AC-coupled output of the MCT detector and the other from its DC-coupled output. The DC signal was collected before the laser was fired and, after a Fourier transform, constituted the single beam static background spectrum. The AC signal was synchronized to the pulse train of the laser and, after a Fourier transform of each time slice, constituted the dynamic time-resolved IR spectral profile recorded at 25 time delays after each laser pulse. The static spectrum was collected as a time average (200 ms) at each mirror position, while the dynamic spectra were collected as a numerical average of 150 laser pulses at each mirror position. The dynamic interferogram at each time delay was obtained by the manipulation of the full array of kinetic data versus mirror position (volts vs mirror position vs

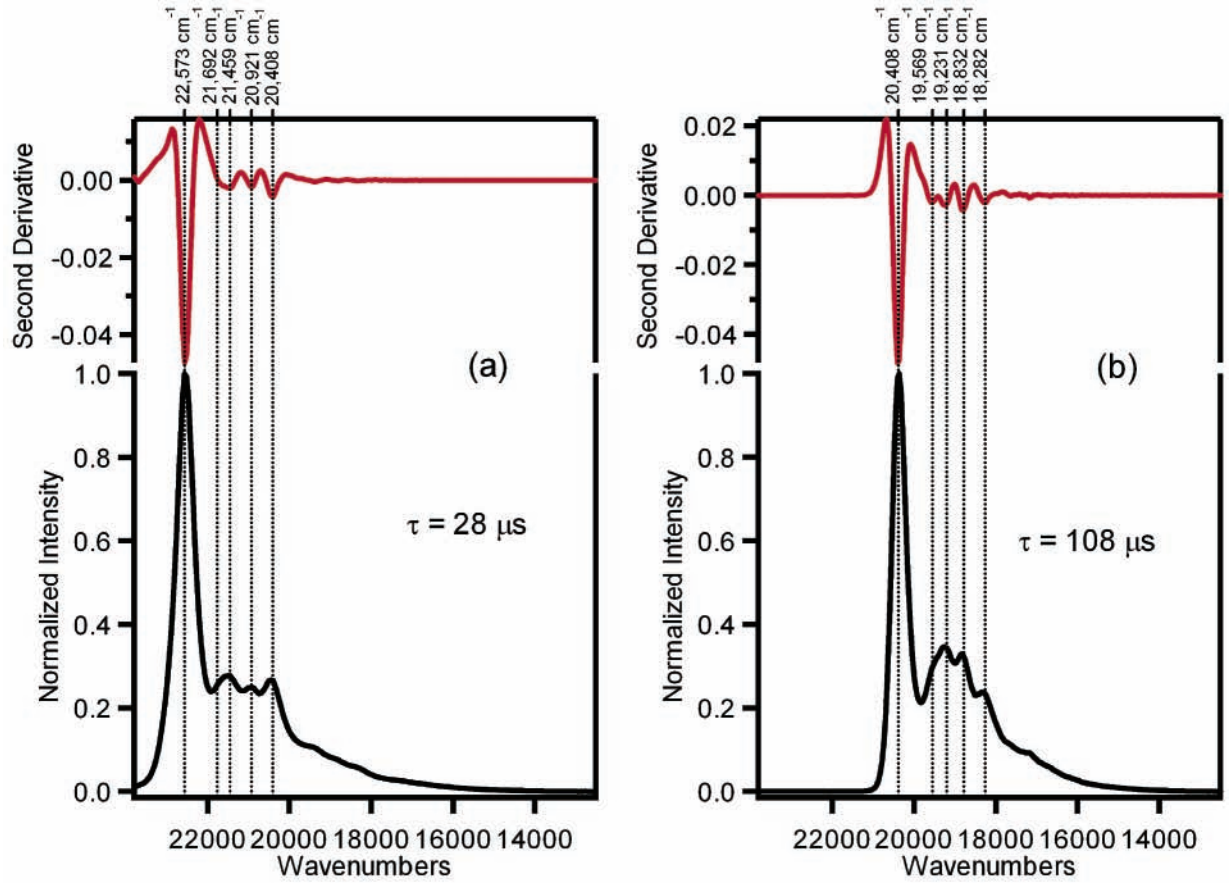

Figure 2. Steady-state emission spectra of (a) Pteb and (b) Ptdeb embedded in PMMA plastic films, cooled to 77 K, and excited with a broad UV band peaking at 360 nm. The red curves above are second derivative spectra used to identify the vibrational fine structure in the steady-state emission spectra.

TABLE 1: Normal Mode Assignments[a] of Most Predominant Peaks[b] Observed in Phosphorescence Spectra

compound	ν_{0-0}	$\nu_{0-0}-\nu_{0-1}$	$\nu_{0-0}-\nu_{0-2}$	$\nu_{0-0}-\nu_{0-3}$	$\nu_{0-0}-\nu_{0-4}$
Pteb	22 573 cm^{-1}	881 cm^{-1}, CH wag on phenyl ring	1114 cm^{-1}, in-plane CH bend on phenyl ring	1652 cm^{-1}, ring stretching mode	2165 cm^{-1}, ethynyl stretch
Ptdeb	20 408 cm^{-1}	839 cm^{-1}, CH wag on phenyl ring	1114 cm, in-plane CH bend on phenyl ring	1611 cm^{-1}, ring stretching mode	2126 cm^{-1}, ethynyl stretch

[a] Assignments based on comparison with vibrational analysis. [b] Frequencies of most prominent peaks are depicted in Figure 2.

time). All time-resolved spectra are plotted as changes in absorbance (ΔA), which is calculated as $\Delta A = \log(1 + \text{dynamic}/\text{static})$ (where dynamic = dynamic single beam spectrum, and static = static single beam spectrum).[17] All spectra reported are the average of five individual experiments.

C. HOMOs, LUMOs, and Frequency Calculations. All quantum mechanical modeling studies employed either Gaussian 98W (version 5.2, revision A.7)[18] or Gaussian 03W[19] software which was implemented on a PC running Microsoft Windows 98 or Microsoft Windows XP as its operating system. The highest occupied molecular orbitals (HOMOs) and lowest unoccupied molecular orbitals (LUMOs), as well as the ground-state vibrational analyses, were determined using optimized geometries. These calculations utilized density functional theory (DFT) with the hybrid B3LYP functional. The basis sets consisted of a standard Gaussian basis (6-31G) on all elements except the platinum metal for which the Stuttgart-Dresden Relativistic Small Core Potential (SDD) was used.[20] For frequency calculations, polarizing functions were added to the lighter elements (6-31G*). All frequencies were corrected with published frequency correction factors.[21−23]

III. Results

A. Luminescence Properties in PMMA at 77 K. The luminescence at 77 K of both Pteb and Ptdeb in PMMA plastics is characterized by a very intense and highly structured phosphorescence. These luminescence spectra are displayed in Figure 2. The curves depicted above each luminescence spectrum are second derivative spectra, which are used as a sensitive method for identifying the positions of peaks and shoulders in the luminescence data. The most prominent features of the luminescence fine structure are listed in Table 1 and are the result of vibrationally excited modes associated with the ethynylbenzene and 1,4-diethynylbenzene ligand(s) attached to the platinum metals. It is important to note that the luminescence bands display vibrational contributions from both the phenyl ring and the ethynyl group(s) of the alkynyl ligands. Second, it is interesting to note that the addition of a single ethynyl group attached to the para position of the benzene ring causes the energy of the phosphorescence band to be shifted by 2208 cm^{-1}. Last, the measured luminescence lifetimes for Pteb and Ptdeb are 28 and 108 μs, respectively.

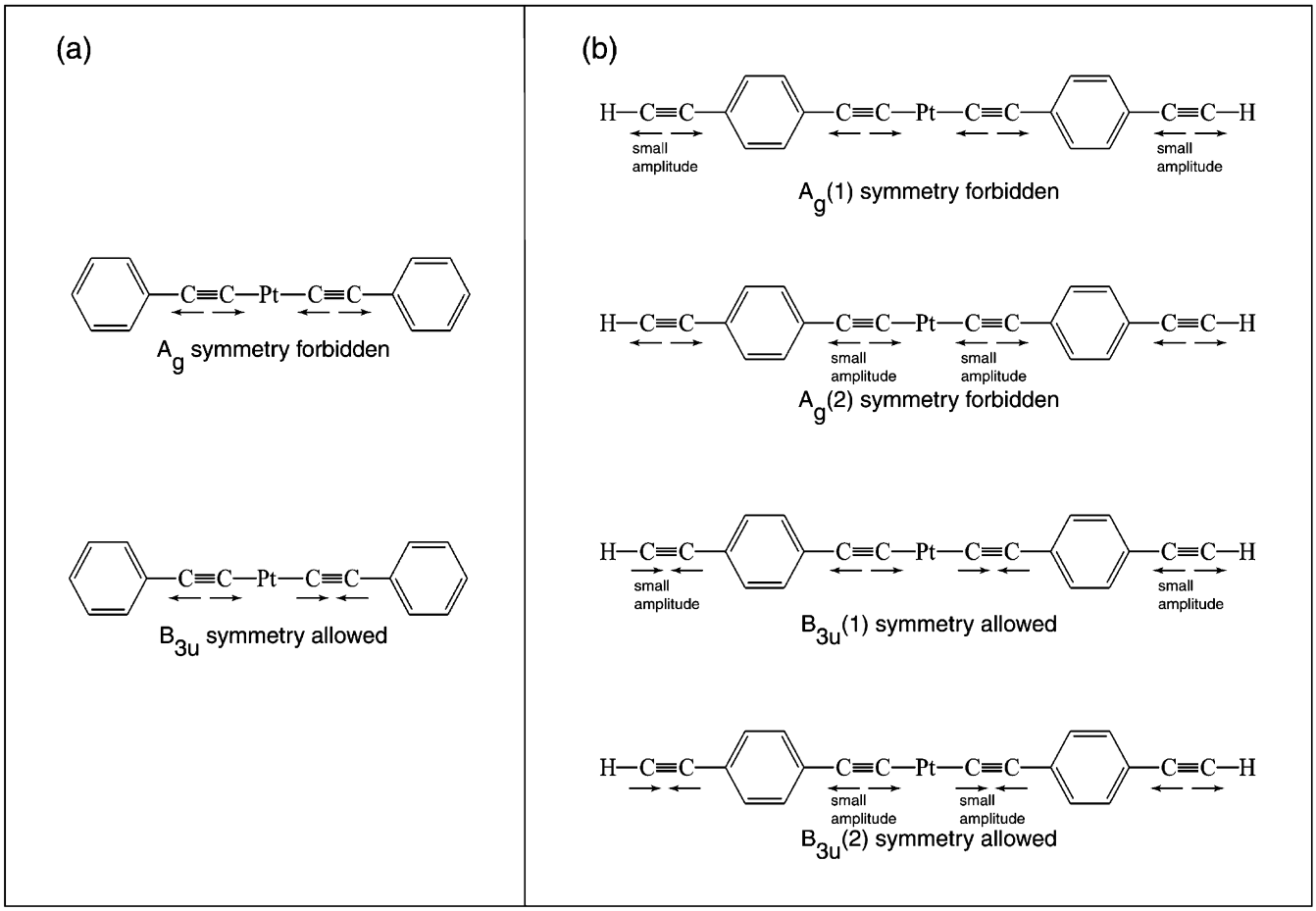

Figure 3. Symmetry assignments for the ethynyl normal modes of vibration for (a) Pteb and (b) Ptdeb. The symmetry labels are based on the D_{2h} point group, and the symmetry selection rules for IR absorption are indicated under each normal mode depicted.

B. Infrared Spectra. The normal modes associated with the ethynyl stretching vibrations for Pteb and Ptdeb are schematically depicted in Figure 3. Figure 3 was derived from a group theoretical analysis (using D_{2h} micro-symmetry) as well as the quantum chemical study described in section II.C. Pteb has two degrees of vibrational freedom associated with the two triple bonds in the molecule: a symmetric A_g stretch, which is IR forbidden, and an antisymmetric B_{3u} stretch, which is IR allowed. On the other hand, Ptdeb has two additional triple bonds in the molecule and thus has four total vibrational degrees of freedom associated with the four carbon−carbon triple bonds: two are IR-forbidden symmetric stretches, $A_g(1)$ and $A_g(2)$, and two are IR-allowed antisymmetric stretches, $B_{3u}(1)$ and $B_{3u}(2)$. The $B_{3u}(1)$ mode has most of its vibrational amplitude associated with the carbon−carbon triple bonds directly attached to the Pt metal. The $B_{3u}(2)$ mode has most of its vibrational amplitude associated with the carbon−carbon triple bonds farthest away from the central platinum metal. The quantum mechanical analysis has predicted that the $B_{3u}(1)$ mode will have a greater infrared absorbance than that of the $B_{3u}(2)$ mode by a factor of about 10.

The ground-state IR spectra in the carbon−carbon triple bond stretching region of Pteb and Ptdeb in PMMA at 77 K are depicted in Figures 4b and 5b. Pteb displays a single mildly intense absorption at 2106 cm^{-1}, and Ptdeb displays a mildly intense absorption at 2096 cm^{-1}. On the basis of the group theoretical and vibrational analyses, these absorptions have been assigned to the antisymmetric stretches associated with the triply bonded carbons that are directly attached to the Pt metals: the B_{3u} mode for Pteb and the $B_{3u}(1)$ mode for Ptdeb.

C. Excited-State Infrared Signatures. The dynamic TRIR data were collected through the AC-coupled output of the MCT detector which only records IR signatures that change in response to the applied laser excitation, which is, in turn, synchronized to the digital storage oscilloscope. Static IR absorptions are silent. Therefore, the TRIR spectra can be interpreted in terms of a change in optical density vs time. The TRIR data (after a Fourier transform and conversion to ΔA) are displayed in Figures 4a and 5a. In the carbon−carbon triple bond region, the TRIR spectra of both Pteb and Ptdeb display bleaches corresponding to the ground-state antisymmetric modes B_{3u} and $B_{3u}(1)$, respectively. Also observed in both TRIR spectra are the grow-ins of a band that overlaps with the bleach but is shifted to slightly higher frequencies in comparison with the ground state and a grow-in at much lower frequencies. Though there are some striking similarities in the TRIR spectra of Pteb and Ptdeb, there is one very important difference. The low-frequency grow-in in the Pteb TRIR spectrum is 111 cm^{-1} lower in energy than the corresponding transient found in the Ptdeb TRIR spectrum.

D. HOMOs and LUMOs. The scope of the theoretical study was limited to a ground-state vibrational analysis, which has already been discussed in terms of the IR assignments, and the elucidation of the HOMOs and LUMOs to get a better idea of the orbital nature of the lowest triplet state. At the simplest conceptual level the lowest excited electronic configurations (singlet and triplet) can be described as the promotion of a single electron from the HOMO to the LUMO. For both Pteb and Ptdeb the HOMOs are derived from $\pi(p_y)$ orbitals conjugated throughout the phenylethynyl ligands and the $5d_{xy}$ orbital on the

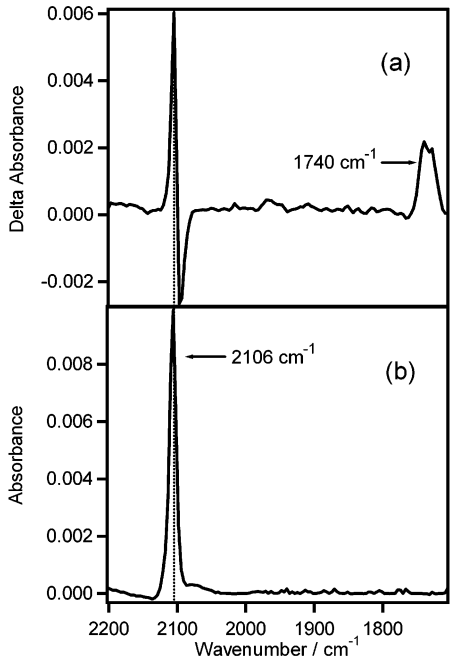

Figure 4. Pteb in PMMA at 77 K: (a) TRIR spectrum, first 5 μs time slice after laser pulse, 355 nm laser excitation, 50 μJ laser pulse, 4 ns pulse width, (b) ground-state FTIR.

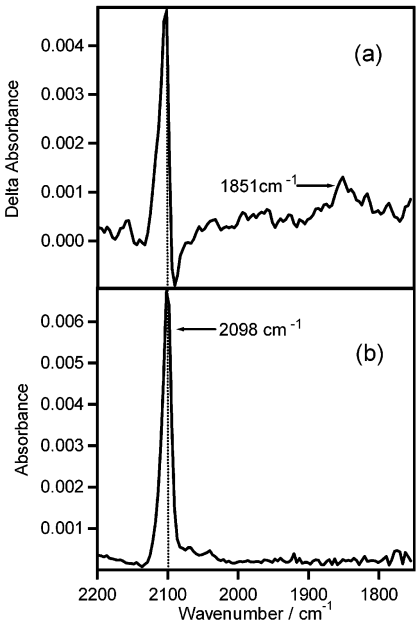

Figure 5. Ptdeb in PMMA at 77 K: (a) TRIR spectrum, first 10 μs time slice after laser pulse, 355 nm laser excitation, 50 μJ laser pulse, 4 ns pulse width, (b) ground-state FTIR.

platinum center. Using the approximate micro-symmetry, D_{2h}, the HOMOs belong to the B_{1g} irreducible representation (Figure 6). Similarly, the LUMOs for both Pteb and Ptdeb are also derived from similar orbital parentages which are primarily $\pi^*(p_y)$ in nature and belong to the B_{2u} irreducible representation. It is also important to note that there is no $5d_{xy}$ character in the LUMOs. Therefore the lowest excited singlet and triplet configurations belong to the $^{1,3}B_{3u}$ irreducible representation and are unique in that they possess both $\pi\pi^*$ and some MLCT character. Careful inspection of the wave functions also shows that the HOMO in Pteb has slightly greater d_{xy} character than that calculated for Ptdeb (36% vs 27%). Therefore it stands to reason that Pteb will have a slightly larger amount of charge-transfer character in its lowest excited triplet than the lowest triplet manifold in Ptdeb. This can account, at least in part, for the shorter lifetime observed for Pteb at 77 K.

IV. Discussion

The nature of the lowest emitting triplet manifold is especially interesting in the context of the current study. It has been shown (Figure 6) that the HOMOs in both Pteb and Ptdeb are π-MOs while the LUMOs are π^* in nature and therefore one can conclude correctly that the phosphorescence in these compounds originate from a spin forbidden $^3\pi\pi^* \rightarrow {}^1$GS transition.[7,13] An interesting point, however, is that the HOMO has a Pt d_{xy} orbital which is directly involved in the π-system and the LUMO has essentially no electron density located on the platinum metal, therefore one could also correctly conclude that the lowest excited triplet manifold is a ^{3}MLCT.[24] The assignments made by Yam *et al.* for similar compounds[9] probably makes the most sense for Pteb and Ptdeb in that the emission originates from a mixed $^3\pi\pi^*/^3$MLCT manifold with predominately intraligand character. This assignment also makes sense in terms of the highly structured phosphorescence spectra (Figure 2) which are typical for emission from either a $^3\pi\pi^*$ or ^{3}MLCT manifold while the observed luminescence lifetimes for Pteb and Ptdeb are intermediate between a typical $^3\pi\pi^*$ and ^{3}MLCT phosphorescence. This assignment brings up an important issue surrounding the symmetry of the excited states of these molecules and has implications for the oligomers and polymers within this family of materials: the issue of symmetry breaking in the excited state. It is well established that in most (if not all) cases involving ^{3}MLCT excited states of high symmetry molecules that the lowest excited manifold results from the promotion of an electron from the metal to only one peripheral ligand (a symmetry-broken excited state).[25−33] A similar question naturally arises for Pteb and Ptdeb, which have both high-symmetry geometries and unusual mixed $^3\pi\pi^*/^3$MLCT excited-state manifolds. Any conclusion regarding a symmetry-broken excited state could also have implications for the observed localized behavior seen in the conjugated organometallic oligomers and polymers of this family.

The current study has used TRIR on the microsecond time scale to directly probe the symmetry properties of the lowest excited manifold. The spectral evidence from the ground-state IR and the excited-state TRIR leads to the conclusion that the symmetry must be reduced in the excited state from D_{2h} to C_{2v} in both Pteb and Ptdeb. This logical conclusion comes from the following argument (for simplicity consider only Pteb). The ground-state IR displays a single IR active mode associated with the antisymmetric stretch of the two carbon−carbon triple bonds, which is B_{3u} under D_{2h} symmetry. If the excited-state retained its D_{2h} symmetry, we would again observed this single IR active mode (B_{3u}), but shifted to a frequency intermediate between a double and triple bond (somewhere between 1800 and 1850 cm^{-1}).[34] However, if the excited state involves only a single ligand, the symmetry will be reduced from D_{2h} to C_{2v} and the IR-allowed B_{3u} mode and the IR-forbidden A_g mode in D_{2h} symmetry will lead to two IR-allowed A_1 modes under C_{2v} symmetry (i.e., all ethynyl normal modes become allowed in C_{2v}). Moreover, the bond order will be reduced for only one of the two carbon−carbon triple bonds and a bifurcated TRIR spectrum will result: one peak for the triple bond on the ligand not associated with the electron promotion and a second peak associated with the excited alkyne ligand of reduced bond order. Clearly the spectral evidence (Figure 4) eliminates the possibility of a symmetry-preserved lowest triplet manifold and proves the

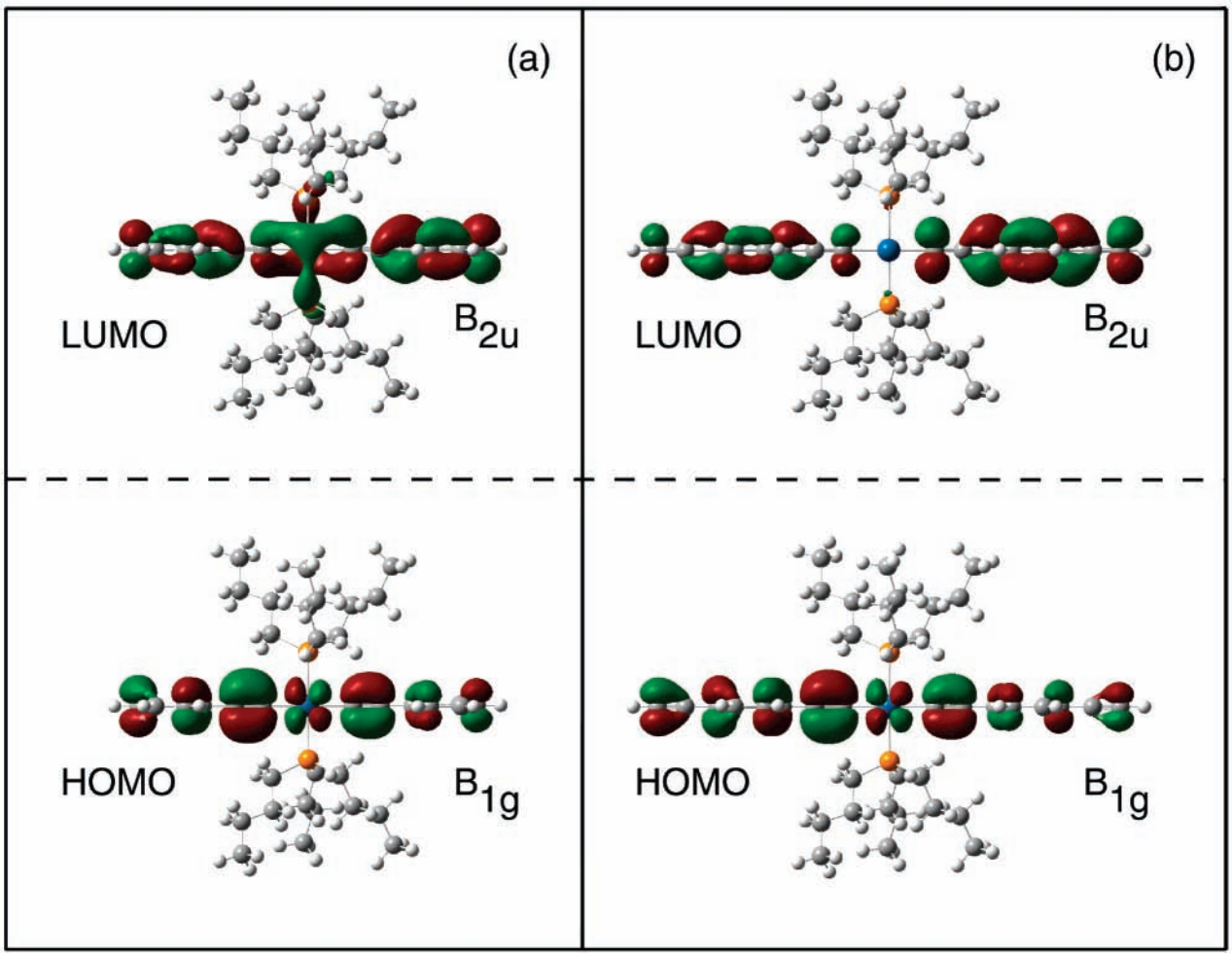

Figure 6. HOMOs and LUMOs derived from DFT/B3LYP study with a 6-31G basis on P, C, and H and the SDD basis on Pt.

symmetry-broken model. Moreover, the excited TRIR spectrum depicted in Figure 4 displays a peak at 1740 cm^{-1}, which is at the high end of what one would expect for a carbon−carbon double bond. Given the HOMO−LUMO for Pteb, this near unity reduction in bond order is reasonable only for a symmetry-broken triplet manifold. Also observed in the TRIR spectrum of Pteb is the grow-in of a peak associated with the carbon−carbon triple bond on the phenylacetylene not involved in the electron promotion of the lowest triplet manifold. This excited-state signature is shifted only slightly to higher frequencies in the excited state and can once again be explained by a careful inspection of the HOMO and LUMO. In the HOMO the d_{xy} orbital is π-antibonded with the π-bonding orbital on the carbon−carbon triple bond. This, in turn, will have the effect of reducing the bond order in the carbon−carbon triple bond slightly. However, in the symmetry-broken excited state the charge density is transferred away from the d_{xy} orbital on the Pt center to only one of the two ligands and the carbon−carbon triple bond order on the ligand that is not excited will be slightly increased. This slight increase in bond order will result in a carbon−carbon triple bond stretch that is shifted to a slightly higher frequency. This is exactly what is observed in the TRIR spectrum. It should be noted that on the microsecond time scale no spectral evidence was observed to support the existence of an initially formed delocalized triplet manifold before the observed reduction in symmetry. This does not exclude the possibility that the initially formed triplet is delocalized, it only means that the symmetry of the lowest excited manifold is already broken on the time scale of the current study. Whether the lowest triplet manifold is initially delocalized and then localizes on a faster time scale or whether the lowest triplet is formed as a localized manifold of states from the very beginning, is still an open question. Eventually this question will need to be addressed with experiments on a much faster time scale than the current study.

The TRIR spectrum of Ptdeb is very similar to the spectrum observed for Pteb with one very important difference. The low-frequency grow-in in the TRIR spectrum of Ptdeb appears at 1851 cm^{-1}, which is 111 cm^{-1} higher in energy than observed for Pteb. Such an observation makes sense only for a symmetry-broken excited state in which the excited electron is spread over the extended π-system of a *single* ligand. In such a case the bond order would be reduced by approximately one-half because the excited electron would be extended over a π^* orbital system containing two acetylene units. Therefore the transient IR signature associated with the excited ligand would fall somewhere between what one would expect for a triple and double bond. This is exactly what we observe in the TRIR spectrum of Ptdeb.

Finally, the phosphorescence spectra need to be reconsidered in terms of a symmetry-broken excited state. The intensity of the fine structure in the luminescence band is indicative of several things related to the electronic structure of the excited state. First, excitations of the vibrational modes associated with the phenyl rings do appear in the luminescence band. This is a clear indication that the excited electron is spread over at least one entire ligand system. Also, because the phosphorescence spectra are so structured, there must be a large equilibrium

internuclear displacement. Taken with the observation that in the lowest triplet manifold the triple-bond order of Pteb is reduced by almost one for only one ligand and in the lowest triplet manifold the triple-bond order of Ptdeb is reduced by almost one-half for one ligand, the largest excited-state distortion is probably along the carbon−carbon triple bond in one of the two ligands, leading to the highly resolved vibrational fine structure in the phosphorescence spectra.

The most fundamental question that arises from this study is why is there excited-state symmetry reduction in the first place? Suppose that in the symmetry-broken excited-state Pteb distorts along the B_{3u} antisymmetric mode and Ptdeb distorts along the antisymmetric $B_{3u}(1)$ mode. Under such a distortion the carbon−carbon triple bond attached directly to the metal is elongated on one ligand and shortened on the other. An elongation of the carbon−carbon triple bond on the excited ligand will stabilize π-antibonded orbitals between acetylenic carbons and a shortening of the carbon−carbon triple bonds will stabilize π-bonded orbitals between acetylenic carbons. Such a distortion naturally stabilizes a symmetry-broken excited state in which half of the molecule will have π-bonded acetylenic carbons and the other half will have π-antibonded acetylenic carbons. Therefore, the coupling between the lowest $^3B_{3u}$ excited triplet manifold with an antisymmetric B_{3u} vibrational mode can result in an energy-stabilized symmetry-broken excited state.

V. Conclusions

A comparison of the ground-state IR spectra and excited-state TRIR spectra of Pteb and Ptdeb has led to the conclusion that the symmetry of both molecules has been reduced from D_{2h} to C_{2v} in which only one of the two ligands is involved in the electronic excitation. With simple inspection of the HOMOs and LUMOs, one can rationalize that a reduction of symmetry along an antisymmetric B_{3u} vibration involving the acetylenic stretch can result in a net stabilization of the lowest $^3B_{3u}$ excited-state manifold. It is observed that the vibrational fine structure in the phosphorescence spectra includes phenyl vibrations along with the acetylenic stretch. Considering this fact along with the fact that the carbon−carbon triple bond stretch in the TRIR spectrum of Ptdeb is higher in frequency by 111 cm^{-1} in comparison with Pteb, it is clear that the excited electron is spread over the entire π-system of a single ligand.

Acknowledgment. The authors acknowledge a grant from the DOE (Office of Science) for support of this research. The University of New Mexico and Los Alamos National Laboratory are also thanked for programmatic support.

References and Notes

(1) Dray, A. E.; Rachel, R.; Saxton, W. O.; Lewis, J.; Khan, M. S.; Donald, A. M.; Friend, R. H. *Macromolecules* **1992**, *25*, 3473−3479.

(2) Fratoddi, I.; Battocchio, C.; Furlani, A.; Mataloni, P.; Polzonetti, G.; Russo, M. V. *J. Organomet. Chem.* **2003**, *674*, 10−23.

(3) Johnson, B. F. G.; Kakkar, A. K.; Khan, M. S.; Lewis, J.; Dray, A. E.; Friend, R. H.; Wittmann, H. F. *J. Mater. Chem.* **1991**, *1*, 485−486.

(4) Lewis, J.; Khan, M. S.; Kakkar, A. K.; Johnson, B. F. G.; Marder, T. B.; Fyfe, B.; Wittmann, H. F.; Friend, R. H.; Dray, A. E. *J. Organomet. Chem.* **1992**, *425*, 165−176.

(5) Rogers, J. E.; Cooper, T. M.; Fleitz, P. A.; Glass, D. J.; McLean, D. G. *J. Phys. Chem. A* **2002**, *106*, 10108−10115.

(6) Walters, K. A.; Dattelbaum, D. M.; Ley, K. D.; Schoonover, J. R.; Meyer, T. J.; Schanze, K. S. *Chem. Commun.* **2001**, *18*, 1834−1835.

(7) Wittmann, H. F.; Friend, R. H.; Khan, M. S.; Lewis, J. *J. Chem. Phys.* **1994**, *101*, 2693−2698.

(8) Yam, V. W. W. *Acc. Chem. Res.* **2002**, *35*, 555−563.

(9) Yam, V. W. W.; Tao, C. H.; Zhang, L.; Wong, K. M. C.; Cheung, K. K. *Organometallics* **2001**, *20*, 453−459.

(10) Wilson, J. S.; Dhoot, A. S.; Seeley, A. J. A. B.; Khan, M. S.; Köhler, A.; Friend, R. H. *Nature* **2001**, *413*, 828−831.

(11) Baldo, M. A.; O'Brien, D. F.; You, Y.; Shoustikov, A.; Sibley, S.; Thompson, M. E.; Forrest, S. R. *Nature* **1998**, *395*, 151−154.

(12) Beljonne, D.; Wittmann, H. F.; Köhler, A.; Graham, S.; Younus, M.; Lewis, J.; Raithby, P. R.; Khan, M. S.; Friend, R. H.; Brédas, J. L. *J. Chem. Phys.* **1996**, *105*, 3868−3877.

(13) Liu, Y.; Shujun, J.; Glusac, K.; Powell, D. H.; Anderson, D. F.; Schanze, K. S. *J. Am. Chem. Soc.* **2002**, *124*, 12412−12413.

(14) Wilson, J. S.; Wilson, R. J.; Friend, R. H.; Kohler, A.; Al-Suti, M. K.; Al-Mandhary, M. R. A.; Kahn, M. S. *Phys. Rev. B* **2003**, *67*, 125206.

(15) Sonogashira, K.; Fujikura, Y.; Yatake, T.; Toyoshima, N.; Takahashi, S.; Hagihara, N. *J. Organomet. Chem.* **1978**, *145*, 101−108.

(16) Hus, C. Y.; Leshner, B. T.; Orchin, M. *Inorg. Synth.* **1979**, *19*, 114−116.

(17) Chen, P.; Palmer, R. A. *Appl. Spectrosc.* **1997**, *51*, 580−583.

(18) Frisch, M. J.; Trucks, G. W.; Schlegel, H. B.; Scuseria, G. E.; Robb, M. A.; Cheeseman, J. R.; Zakrzewski, V. G.; Montgomery, J. A., Jr.; Stratmann, R. E.; Burant, J. C.; Dapprich, S.; Millam, J. M.; Daniels, A. D.; Kudin, K. N.; Strain, M. C.; Farkas, O.; Tomasi, J.; Barone, V.; Cossi, M.; Cammi, R.; Mennucci, B.; Pomelli, C.; Adamo, C.; Clifford, S.; Ochterski, J.; Petersson, G. A.; Ayala, P. Y.; Cui, Q.; Morokuma, K.; Salvador, P.; Dannenberg, J. J.; Malick, D. K.; Rabuck, A. D.; Raghavachari, K.; Foresman, J. B.; Cioslowski, J.; Ortiz, J. V.; Baboul, A. G.; Stefanov, B. B.; Liu, G.; Liashenko, A.; Piskorz, P.; Komaromi, I.; Gomperts, R.; Martin, R. L.; Fox, D. J.; Keith, T.; Al-Laham, M. A.; Peng, C. Y.; Nanayakkara, A.; Challacombe, M.; Gill, P. M. W.; Johnson, B.; Chen, W.; Wong, M. W.; Andres, J. L.; Gonzalez, C.; Head-Gordon, M.; Replogle, E. S.; Pople, J. A. *Gaussian*, A.7 ed.; Gaussian: Pittsburgh, 2001.

(19) Frisch, M. J.; Trucks, G. W.; Schlegel, H. B.; Scuseria, G. E.; Robb, M. A.; Cheeseman, J. R.; Montgomery, J. A.; Vreven, T.; Kudin, K. N.; Burant, J. C.; Millam, J. M.; Iyengar, S. S.; Tomasi, J.; Barone, V.; Mennucci, B.; Cossi, M.; Scalmani, G.; Rega, N.; Petersson, G. A.; Nakatsuji, H.; Hada, M.; Ehara, M.; Toyota, K.; Fukuda, R.; Hasegawa, J.; Ishida, M.; Nakajima, T.; Honda, Y.; Kitao, O.; Nakai, H.; Klene, M.; Li, X.; Knox, J. E.; Hratchian, H. P.; Cross, J. B.; Adamo, C.; Jaramillo, J.; Gomperts, R.; Stratmann, R. E.; Yazyev, O.; Austin, A. J.; Cammi, R.; Pomelli, C.; Ochterski, J. W.; Ayala, P. Y.; Morokuma, K.; Voth, G. A.; Salvador, P.; Dannenberg, J. J.; Zakrzewski, V. G.; Dapprich, S.; Daniels, A. D.; Strain, M. C.; Farkas, O.; Malick, D. K.; Rabuck, A. D.; Raghavachari, K.; Foresman, J. B.; Ortiz, J. V.; Cui, Q.; Baboul, A. G.; Clifford, S.; Cioslowski, J.; Stefanov, B. B.; Liu, G.; Liashenko, A.; Piskorz, P.; Komaromi, I.; Martin, R. L.; Fox, D. J.; Keith, T.; Al-Laham, M. A.; Peng, C. Y.; Nanayakkara, A.; Challacombe, M.; Gill, P. M. W.; Johnson, B.; Chen, W.; Wong, M. W.; Gonzalez, C.; Pople, J. A. *Gaussian*, Revision of A.1 ed.; Gaussian: Pittsburgh, 2003.

(20) Basis sets were obtained from the Extensible Computational Chemistry Environment Basis Set Database, V., as developed and distributed by the Molecular Science Computing Facility, Environmental and Molecular Sciences Laboratory which is part of the Pacific Northwest Laboratory, P.O. Box 999, Richland, WA 99352, USA, and funded by the U.S. Department of Energy. The Pacific Northwest Laboratory is a multi-program laboratory operated by Battelle Memorial Institute for the U.S. Department of Energy under contract DE-AC06−76RLO 1830. Contact David Feller or Karen Schuchardt for further information.

(21) Pople, J. A.; Scott, A. P.; Wong, M. W.; Radom, L. *Israel J. Chem.* **1993**, *33*, 345−350.

(22) Scott, A. P.; Radom, L. *J. Phys. Chem.* **1996**, *100*, 16502−16513.

(23) Wong, M. W. *Chem. Phys. Lett.* **1996**, *256*, 391−399.

(24) Sacksteder, L. A.; Baralt, E.; DeGraff, B. A.; Lukehart, C. M.; Demas, J. N. *Inorg. Chem.* **1991**, *30*, 2468−2476.

(25) Yeh, A. T.; Shank, C. V.; McCusker, J. K. *Science* **2000**, *289*, 935−938.

(26) Damrauer, N. H.; Weldon, B. T.; McCusker, J. K. *J. Phys. Chem. A* **1998**, *102*, 3382−3397.

(27) Damrauer, N. H.; Cerullo, G.; Yeh, A. T.; Boussie, T. R.; Shank, C. V.; McCusker, J. K. *Science* **1997**, *275*, 54−57.

(28) Bradley, P. G.; Kress, N.; Hornberger, B. A.; Dallinger, R. F.; Woodruff, W. H. *J. Am. Chem. Soc.* **1981**, *103*, 7441−7446.

(29) Forster, M.; Hester, R. E. *Chem. Phys. Lett.* **1981**, *81*, 42−47.

(30) Gold, J. S.; Milder, S. J.; Lewis, J. W.; Kliger, D. S. *J. Am. Chem. Soc.* **1985**, *107*, 8285−8286.

(31) Carroll, P. J.; Brus, L. E. *J. Am. Chem. Soc.* **1987**, *109*, 7613−7616.

(32) Kober, E. M.; Sullivan, B. P.; Meyer, T. J. *Inorg. Chem.* **1984**, *23*, 2098−2104.

(33) Riesen, H.; Wallace, L.; Krausz, E. *Inorg. Chem.* **1996**, *35*, 6908−6909.

(34) Colthup, N. B. *J. Opt. Soc. Am.* **1950**, *40*, 397−400.